

Driving with temperature the synthesis of graphene films and nanoribbons on Ge(110)

L. Persichetti¹, M. De Seta^{1,*}, A. M. Scaparro¹, V. Miseikis², A. Notargiacomo³, A. Ruocco¹, A. Sgarlata⁴, M. Fanfoni⁴, F. Fabbri⁵, C. Coletti², and L. Di Gaspare¹

¹*Dipartimento di Scienze, Università Roma Tre, Viale G. Marconi, 446- 00146 Rome, Italy*

²*Center for Nanotechnology Innovation @NEST, IIT, Piazza San Silvestro 12, 56127 Pisa, Italy*

³*Institute for Photonics and Nanotechnology, Via Cineto Romano 42, 00156, CNR-Rome, Italy*

⁴*Dipartimento di Fisica, Università di Roma "Tor Vergata", Via Della Ricerca Scientifica, 1- 00133 Rome, Italy*

⁵*NEST, Istituto Nanoscienze – CNR, Scuola Normale Superiore, Piazza San Silvestro 12, I-56127 Pisa, Italy.*

By tuning the growth parameters, we show that it is possible to drive the CVD synthesis of graphene on Ge(110) towards the formation of either ultrathin armchair nanoribbons or of continuous graphene films. The ribbons are aligned along specific high-symmetry directions of the Ge(110) surface and have a width of ~5 nm. Moreover, by merging spectroscopic and morphological information, we find that the quality of graphene films depends critically on the growth temperature improving significantly in a narrow range close to the Ge melting point. The abruptness of the temperature behavior observed indicates that achieving high-quality graphene is intimately connected to the quasi-liquid Ge layer formed close to 930 °C on the substrate. Being observed for diverse Ge orientations, this process, known as incomplete melting, is shown to be of general relevance for graphene synthesis on Ge, and explains why similar growth conditions present in literature lead to graphene of very diverse quality on these substrates.

Keywords: Graphene, Graphene nanoribbons, Germanium, Catalysis, Chemical Vapor Deposition, Scanning Tunneling Microscopy

*corresponding author:

Fax: +39 0657333430 E mail: monica.deseta@uniroma3.it (Monica De Seta)

1. Introduction

The last decade has been marked by extraordinary advances in the field of two-dimensional (2D) materials made possible by the discovery of graphene [1]. This category of materials is characterized by an unprecedented wealth of attractive and excellent properties and functionalities that can be further tuned by confinement effects, as in graphene nanoribbons [2, 3]. Therefore, technological application of graphene materials is expected to revolutionize fields, such as electronics and optoelectronics, which are currently dominated by group-IV elementary semiconductors, i.e. Si and Ge. To unlock this potential, a critical and necessary breakthrough is the integration of graphene films and nanostructures with the complementary metal-oxide-semiconductor (CMOS) manufacturing process of semiconductors [4]. To date, the main obstacle to the integration and CMOS compatibility [5] is the metallic contamination introduced in the graphene during the metal-catalyzed deposition process or film transfer. Alternative synthetic approaches, such as the unzipping of carbon nanotubes typically used for obtaining sub-10 nm graphene nanoribbons and flakes [6-8], suffer from the same issue, due to contamination by metal nanoparticles originating from the growth process of nanotubes. Thanks to the catalytic activity of Ge on gaseous carbon precursors combined with Ge carbides instability, chemical vapor deposition (CVD) of graphene on Ge or Ge/Si substrates represents a viable growth route [9-15] for obtaining metal-free, CMOS-compatible graphene. After the seminal works by Wang *et al.* [9] and Lee *et al.* [10] on Ge(110), most of the attention has been focused on the Ge(001) surface, this being, in principle, the most technologically relevant one. On this face, the growth of high-quality graphene has already been demonstrated [13, 16-20], as well as the synthesis by CVD of ultra-thin ribbons having widths narrower than 5 nm [21-25]. Experiments have also shown, however, that the Ge(001) surface under the graphene flakes or ribbons is severely faceted along $\{1,0,L\}$ orientations [11, 13, 16, 21, 26, 27], consistent with the existence of several surface-energy minima around the Ge(001) face which favor faceting at high temperature [28, 29] or under strain [30]. The nanofaceting development questioned the suitability of

this interface for further technological processing, and has led to renewed interest in graphene/Ge(110) for which the underlying Ge surface not only remains flat but also promotes the formation of a graphene single crystal [10]. Attention has been focused on the electronic properties of graphene grown on Ge(110) [15, 31] and on the interfacial structure with the Ge surface [32-35], revealing at the interface both structural motifs related to the (1x1) Ge termination [33] and a characteristic (6x2) Ge reconstruction [32, 34, 35] which is not observed for bare Ge(110) without graphene. Morphologically, the growth of uniaxially aligned graphene islands [36] merging into a uniform graphene film [37] has been observed, whereas no nanoribbon formation has yet been reported so far, in contrast to the Ge(001) substrate. Here, we show that, by tuning the annealing temperature of Ge(110) substrate during the pre-growth procedure and the CVD deposition temperature of graphene, we are able to direct the growth process either towards the synthesis of ultrathin armchair nanoribbons or towards a continuous graphene film. The ribbons are aligned along specific high-symmetry directions of the Ge(110) surface and have a width of ~5 nm, this being a size level of interest for high-performance digital electronics [22]. Moreover, by merging spectroscopic and morphological information, we find that close to the Ge melting point the quality of graphene films depends critically on the growth temperature and improves significantly by increasing the deposition temperature in the 910-930 °C range. This indicates that the quasi-liquid Ge layer formed at about 930 °C (incomplete melting) plays a critical role for obtaining high-quality graphene on Ge(110). Reported first on Ge(001) [20], the correlation between incomplete melting of Ge and the quality of graphene synthesis is shown here to be of a general relevance for graphene synthesis on Ge substrates.

2. Materials and methods

Graphene and graphene nanoribbons were grown on Ge(110) substrates (*n*-type Sb-doped, $n=10^{16}$ cm⁻³) using a commercial CVD reactor (Aixtron BM). Ge substrates were cleaned *ex-situ* by multiple rinsing and drying cycles alternating isopropyl alcohol and de-ionized water followed by an *in-situ* annealing to

temperature T_C in H₂/Ar atmosphere without methane. Deposition of graphene was performed at 100 mbar from a CH₄/H₂ gas mixture using Ar as carrier gas. For CH₄, H₂ and Ar, the fluxes were set at 2, 200, and 800 sccm, respectively. The deposition temperature T_D was varied between 890 and 930 °C and, after the growth, samples were cooled down to room temperature in H₂ and Ar atmosphere. For substrate heating, we adopted a multi-step temperature ramp with a rate progressively decreasing close to the target temperature. Such a procedure ensured accurate control over the temperature close to the Ge melting point.

The graphene samples were characterized by using X-rays photoelectron (XPS) and Raman spectroscopies. The XPS measurements were carried out using a monochromatic Al K_α source ($h\nu=1486.6$ eV) and a concentric hemispherical analyzer operating in retarding mode (Physical Electronics Instruments PHI), with an energy resolution of 0.4 eV. The carbon amount ρ deposited on the samples was estimated from the C_{1s} core level area intensity normalized to that acquired in the same experimental conditions on a commercial graphene monolayer (CGM) positioned next to the analyzed sample, i.e. $\rho = I_{C_{1s}}^{sample} / I_{C_{1s}}^{CGM}$ [18].

Raman spectroscopy was performed with a Renishaw *inVia* confocal Raman microscope using an excitation wavelength of 532 nm, a 100x objective and a laser spot size of 1 μ m. For a quantitative analysis, the intensity ratios of the Raman bands were obtained from the integrated intensity of the fitting peaks.

The sample morphology was investigated by scanning electron microscopy (SEM) (FEI Helios 600 NanolabDualBeam), atomic force microscopy (AFM) (Bruker Dimension Icon microscope) operating in Tapping Mode, and ultra-high-vacuum (UHV), room-temperature scanning tunnelling microscopy (STM) (VT Omicron) working in constant current mode. Finally, low-energy electron diffraction (LEED) was employed for assessing the crystalline quality of graphene. Conventional back-display (*c*-LEED) measurements were paralleled by high-resolution LEED using a monochromatic electron gun

and a hemispherical electron analyzer. Reciprocal space is spanned by the vectorial quantity \mathbf{q} which is the momentum transfer of the diffraction experiment. In the specular (elastic) conditions, the component of \mathbf{q} parallel to the surface vanishes, thus defining the zero-*th* order diffraction peak. By scanning the polar angle θ (while keeping fixed the incidence and collection angles), the scattering vector component parallel to the surface is changed and a surface diffraction peak is observed for $\mathbf{q}_{//}$ matching a surface reciprocal lattice vector. The crystallographic direction probed on the surface is instead defined by the azimuthal orientation ϕ .

3. Results and discussion

Effect of deposition temperature on quality and morphology of graphene monolayers

In a first set of experiments, three graphene samples were deposited at T_D equal to 910, 920 and 930 °C, respectively, using for each sample an annealing temperature T_C equal to T_D (i.e. $T_C = T_D$). The small variations in the deposition temperature produced striking differences in the grown graphene in terms of quality, as evident from Raman spectra in Fig. 1, and morphology at different length scales probed by SEM, AFM and STM (Fig. 2). Note, however, that the total carbon amount ρ measured by XPS data depends very slightly on the temperature (varying less than 15%), being close to 1 for all the samples (see Table 1). This information, together with the absence of extended bilayer regions in SEM images [Fig. 2(a-c)], indicates that a graphene monolayer covers the Ge substrate almost uniformly in all the samples.

T_D (°C)	ρ (graphene monolayers)	Γ_{2D} (cm^{-1})	I_{2D}/I_G	I_D/I_G
910	0.88	48	1.7	2.0
920	0.91	47	2.4	1.5
930	0.99	46	3.0	0.3

Table 1. Quantitative analysis of XPS and Raman spectra.

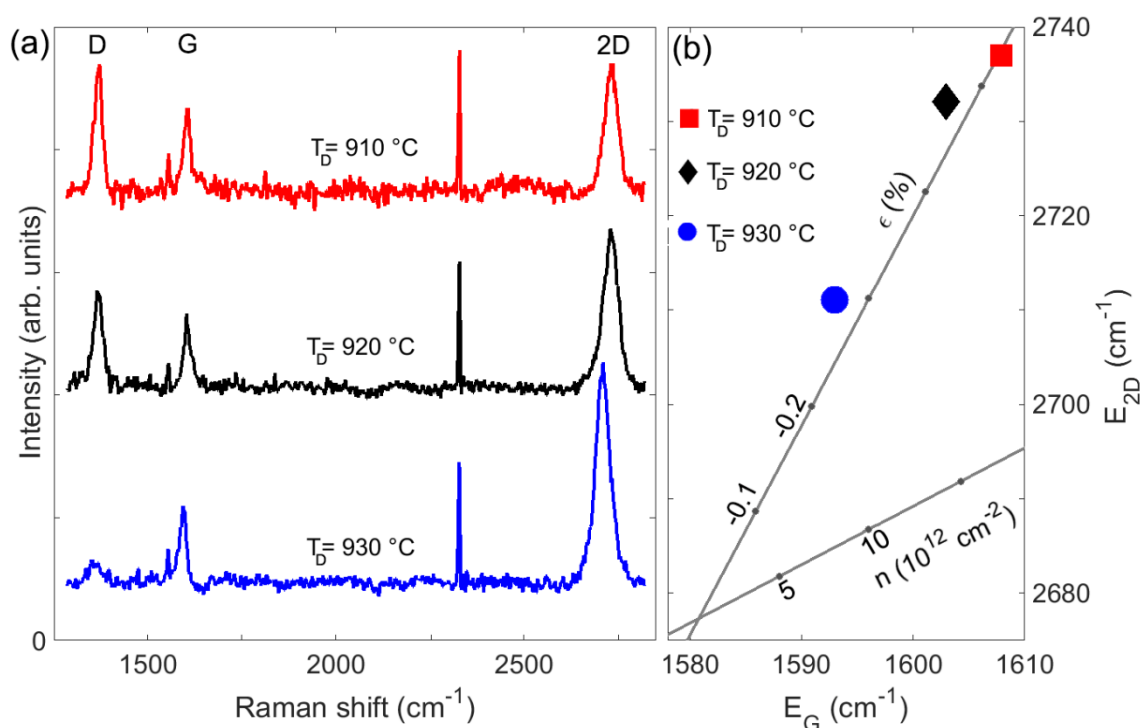


Fig. 1. (a) Raman spectra of graphene samples grown on Ge(110) at different $T_D (=T_C)$. (b) Plot of the 2D- vs G- band energies. ϵ is the strain and n the charge density. Straight lines indicate E_{2D} vs E_G relationship for strained undoped ($n=0$) and unstrained ($\epsilon=0$) n -doped graphene. The two lines cross at the expected 2D and G positions for suspended freestanding single-layer graphene (neutrality point).

In Fig. 1(a), we observe the main Raman features of graphene, i.e. 2D and G bands respectively at ~ 2700 and ~ 1600 cm^{-1} in all the spectra. In addition, the D peak originating from intervalley resonant scattering due to defects is also visible. At higher T_D we observe a boost of the I_{2D}/I_G intensity ratio produced by the increase of the 2D intensity (See Table I) while the width of the 2D peak is almost unaffected by T_D variation. These observations indicate that, in the temperature range explored, an increase of T_D as low as 20 $^{\circ}\text{C}$ produces a major improvement in the crystalline quality of the graphene film [38-40]. Accordingly, we observe that the I_D/I_G ratio drops upon increasing T_D , suggesting an effective reduction in the defect concentration at high temperature.

By analyzing the diagram of the 2D vs G band energies [Fig. 1(b)], one can compare the strain and doping levels of the three graphene samples [41]. We find that the doping density is almost independent of the growth temperature T_D , this being, in line with previous observations [11], negligible on Ge(110). The strain, instead, shows a clear dependence on T_D . As the deposition temperature gets higher, it decreases from the value of -0.52 % at $T_D= 910$ $^{\circ}\text{C}$ to less than -0.3 % at 930 $^{\circ}\text{C}$. The origin of this compressive strain is likely related to different thermal expansion coefficients (CTEs) of graphene [42] and Ge [43]. While at the deposition temperature the CTE of graphene is larger than that of Ge, below ~ 500 $^{\circ}\text{C}$ graphene CTE becomes rapidly smaller than that of the substrate: this means that a compressive thermal strain is built up in graphene during cooling, as observed by Raman spectroscopy [16]. Previous work showed that such a strain can be effectively reduced by formation of wrinkles in graphene [44]. By comparing the SEM images in Figs. 2(a-c), it is evident that, while no wrinkles are observed at $T_D= 910$ $^{\circ}\text{C}$ (i.e. where the strain is larger), a wrinkle pattern does appear at $T_D= 920$ $^{\circ}\text{C}$ and 930 $^{\circ}\text{C}$. In the two samples the wrinkle edges have almost the same directions and form 120° angles. The tessellation areas defined by the wrinkle pattern widen markedly between 920 and 930 $^{\circ}\text{C}$, showing at the highest temperature longer edges and a more homogeneous distribution over the surface. From AFM [Figs. 2(d-f)], it is also found that the wrinkle height increases with temperature, from ~ 1.5 nm at 920 $^{\circ}\text{C}$ to ~ 3 nm

at 930 °C. Based on these observations, it is reasonable to hypothesize that the higher and more uniformly distributed wrinkles at 930 °C are capable of better relieving the thermal strain, so explaining the higher degree of relaxation measured by Raman spectra at this temperature.

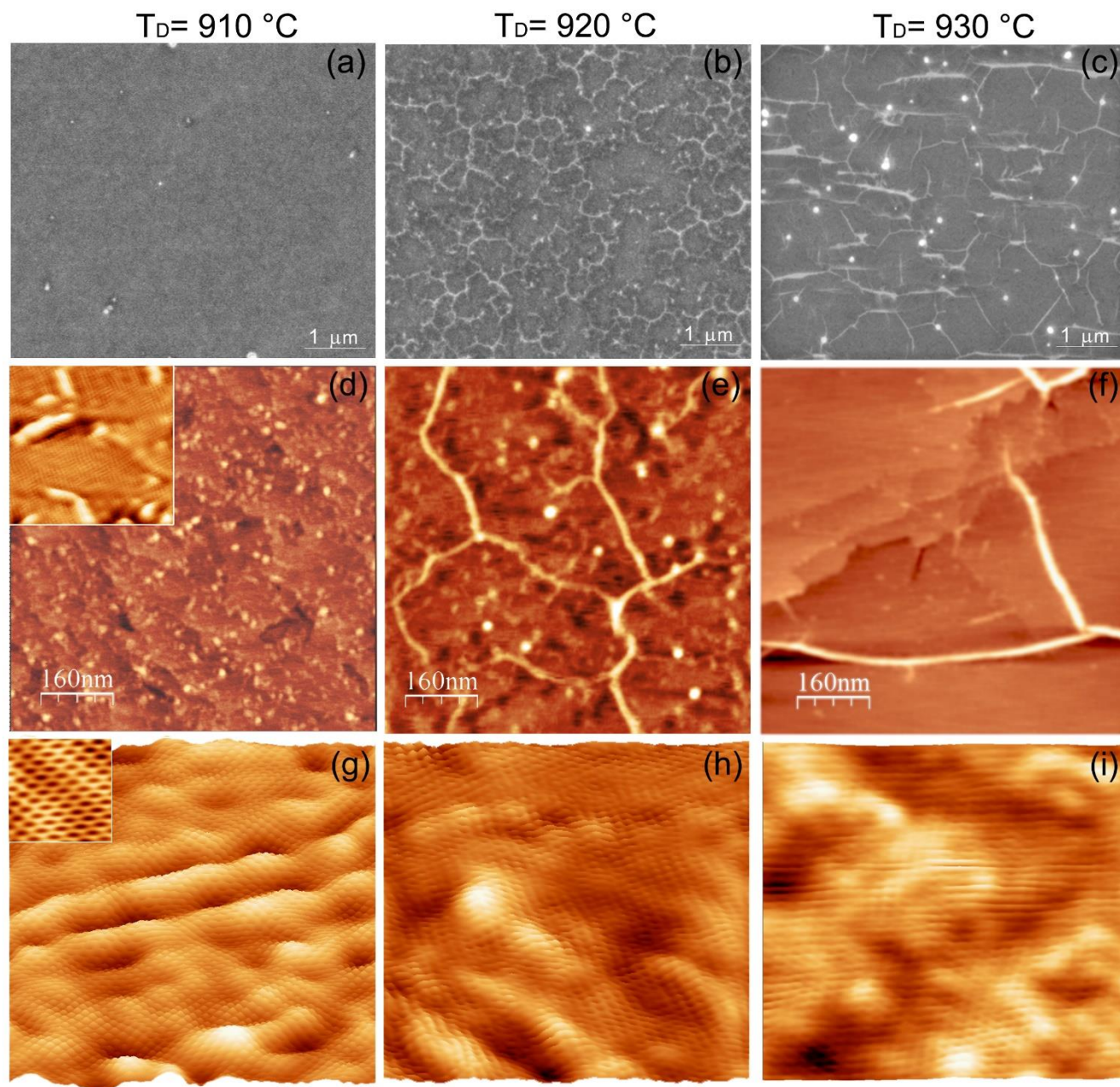


Fig. 2. Morphological characterization of graphene films grown on Ge(110) at different $T_D (=T_C)$. (a-c) SEM images. (d-f) AFM images. The maximum of the z axis increases from (d) to (f) being,

respectively, 0.9 nm, 1.8 nm and 3.2 nm. In the inset of panel (d), a STM image (50x 50) nm² is shown. (g-i) 3D STM topographies (8.2x 8.2) nm² displayed with the same z-axis range 0-0.12 nm. In the inset of panel (g), a (1.3x 1.3) nm² blow-up of the honeycomb lattice is displayed. STM images were taken with the following tunneling parameters $U= 50$ mV, $I=1.0$ nA.

In addition to the presence/absence of wrinkles, the AFM topographies shown in Figs. [2(d-f)] reveal that the morphology of the Ge substrate also changes dramatically with temperature. Despite the fact that the typical terrace/step structure of the Ge surface is visible in all the samples, the terrace widths increase markedly with temperature, being <70 nm at $T_D= 910$ °C and reaching several hundreds of nanometers at 930 °C. In addition, in the samples grown below 930 °C we note the presence of defects which appear as bumps or ridges in AFM measurements. The density of such defects is particularly high on the sample deposited at $T_D= 910$ °C [Fig. 2(d)]. Their structure is better clarified by STM imaging [inset Fig. 2(d)] which shows worm-like ridges and rounded bumps with a lateral size of a few nanometers and heights ranging between 0.3-0.5 nm. Moreover, it is evident that the graphene layer covers continuously the substrate, following the corrugation of the ridges. Among the ridges, graphene is not completely flat but shows a rippling pattern with a typical wavelength of ~1 nm. This ripple morphology present at low T_D is better evident at higher magnification [Figs. 2(g-h)]. We found in the sample deposited at $T_D = 910$ °C a root-mean-square (RMS) roughness R_q equal to 0.55 Å, while, at higher T_D , graphene becomes definitely flatter, with the roughness being more than halved at 930 °C ($R_q= 0.21$ Å).

Further investigation of the graphene sample deposited at $T_D= 930$ °C is reported in Fig. 3. High-resolution STM images show a clear-cut honeycomb lattice extending over wide flat areas and resulting in an undistorted six-fold pattern obtained by fast-Fourier transform (FFT) [Figs. 3(a-c)]. On a larger scale [Fig 3 (d)], besides the presence of the Ge terraces and steps, STM images show small nuclei of graphene bilayer with a Moiré superlattice of ~4.38 nm periodicity [Fig 3 (e)]. From this value [45], we

evaluate a misorientation angle between the two stacked graphene layers of about 3.2° . Considering that the bilayer nuclei are detected on a minority of STM sampling, we estimate the bilayer coverage to be $< 2\%$. Interestingly, by changing the bias voltage, STM probes the Ge surface underneath the graphene. In

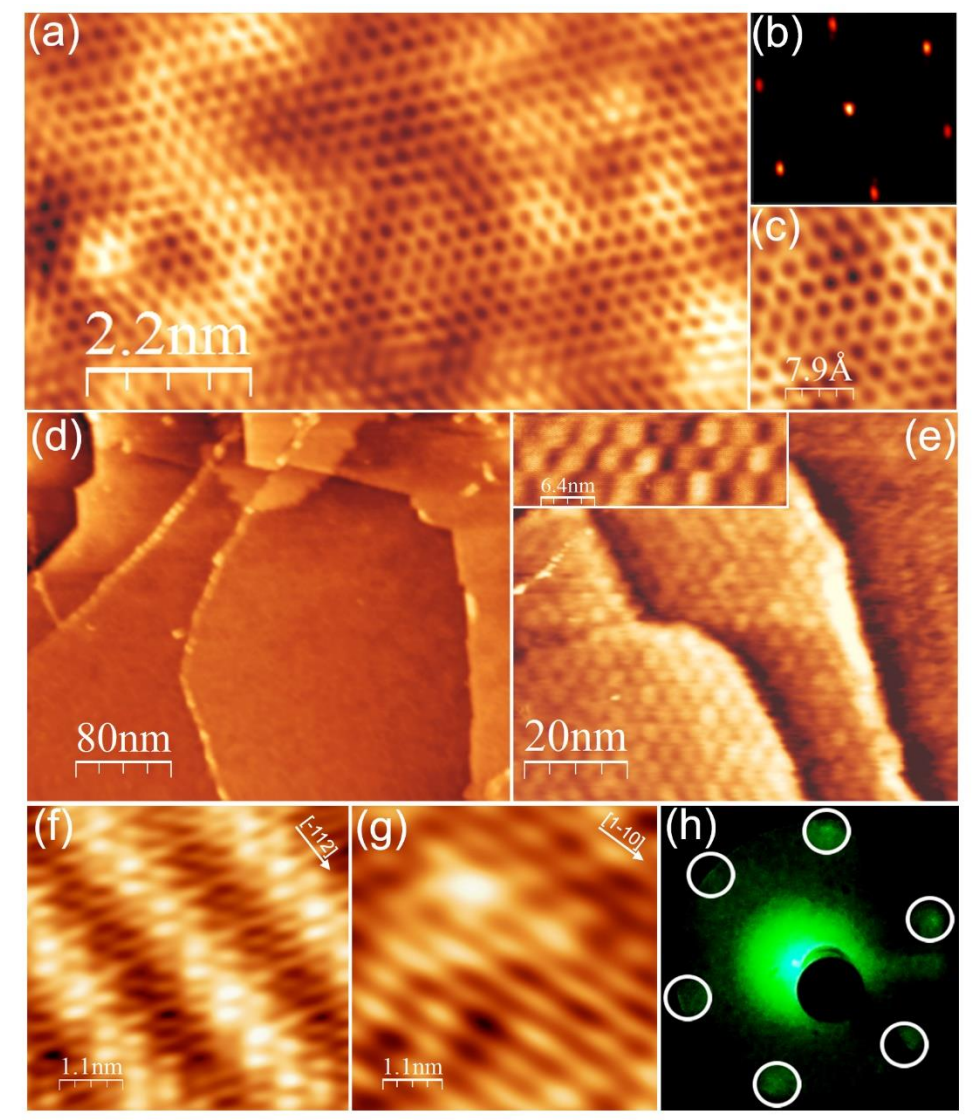


Fig. 3. Graphene sample deposited at $T_D = T_C = 930^\circ\text{C}$: (a) honeycomb lattice of graphene monolayer. (b) FFT of the STM image and (c) enlarged view of graphene lattice. (d) large-scale STM picture of an area of the sample where a bilayer graphene is present in the center-top part of the image. (e) enlarged views of the bilayer graphene showing a Moiré superlattice. On the right-most terrace, a monolayer graphene is present. STM images of (f) (6x2) reconstruction and (g) (1x1)-termination of

the Ge(110) surface under the graphene monolayer. (h) c-LEED image. STM images in panels (f) and (g) were acquired with $U = -2.2$ V, $I = 0.5$ nA, all the others with $U = 50$ mV, $I = 1.0$ nA.

line with previous results [33], we find the coexistence of areas with different Ge surface patterns: zones showing a superstructure with a periodicity of about 1.7 nm [Fig. 3(f)] are alternated with areas where atomic rows with a much thinner spacing of ~ 0.55 nm are observed [Fig. 3(g)]. The former structure has been attributed to the (6x2) reconstruction of Ge(110) below the graphene. This reconstruction has not been observed for bare Ge(110), its being peculiar to the graphene/Ge system [33-35, 45]. Instead, the origin of structural motif in Fig. 3(g) is still being debated [33, 35]. The spacing observed between atomic rows is consistent with that of the unreconstructed (1x1) Ge(110) surface along the [001] direction (which is indeed the direction perpendicular to the rows). Therefore, it has been suggested that the surface pattern is due to the (1x1) bulk termination of Ge(110) stabilized by hydrogen present in the growth environment of CVD graphene [33]. However, it has been also proposed that the same structure can be interpreted as a diverse, novel surface reconstruction of Ge(110) strongly interacting with graphene and formed by post-growth UHV annealing to $T > 800$ °C [35]. We note that no such a treatment was performed on our samples; nonetheless, we mostly observe the typical pattern of Fig. 3(g), whereas the (6x2) reconstruction [Fig. 3(f)] is observed only locally, on less than 10% of the surface.

Structurally, the high-quality of the graphene film for $T_D = 930$ °C is confirmed by LEED. Figure 3(h) shows the conventional c-LEED pattern of the 930 °C sample. Only one set of hexagonally arranged diffraction spots are detected on the fluorescence screen, indicating that graphene is mostly single crystal. To obtain more quantitative information, we performed high-resolution LEED measurements by using a hemispherical electron analyzer (Fig. 4); the geometry of the setup is sketched in the inset. For $\phi = 0^\circ$ the sample is aligned in the Γ -M direction (dark blue curve in Fig. 4). An ideal single-crystal graphene would show an individual reflection corresponding to $\mathbf{q} // \mathbf{G}_{\Gamma\text{-M}}$, which could also be visible in

different diffraction orders. In our case this peak (with its second-order replica) is dominant, but we also observe an additional shallow feature. By changing the azimuth, we find that the intensity of this feature shows a maximum for $\phi = 30^\circ$, i.e. when the azimuth is oriented along the Γ -K direction [light blue curve]. This reflection could be due to a minority of graphene domains with different crystalline orientation rotated by 30° with respect to the dominant one. The formation of such domains has been observed in the literature [15] as an additional subset of spots rotated by 30° in *c*-LEED. In contrast, in our case, these spots are not visible in *c*-LEED, indicating that this second orientational domain is clearly marginal. Indeed, from the intensity ratio between the Γ -M and Γ -K peaks in Fig. 4, we estimate the abundance of the minor orientation to be $<10\%$. We remark that the Γ -K diffraction peak cannot be due to the second graphene layer, since the misorientation angle between the two stacked layers obtained from the Moiré superlattice is much lower than 30° .

The data reported in this section demonstrate that the quality of graphene/Ge(110) changes drastically when the deposition temperatures is slightly varied close to the melting point of Ge (938°C). Namely, in our growth conditions, graphene of high quality is obtained at $T_D = 930^\circ\text{C}$ but degrades significantly just 20°C below this setpoint. In analogy with what has been recently observed on Ge(001)[20], we attribute this abrupt behavior to the incomplete surface melting of Ge [46] in which, a *quasi*-liquid Ge surface layer is formed only a few degrees below the melting point. Based on the temperature behavior observed, we believe that the sample deposited at 930°C was grown at a temperature above the onset of the surface-melting regime. Consistently, an abrupt change in the Ge topography occurs in this sample which develops large terrace widths due to the higher diffusivity and weakening of the in-plane bonding of surface Ge atoms in the melted regime. Graphene synthesis on a *quasi*-liquid Ge surface strongly differs from that occurring on a solid substrate. While growing, graphene tends to follow the potential energy minimum of the van der Waals interaction [47]: the presence of a mobile, liquid Ge layer hinders strong surface corrugations of the substrate, thus preventing the rippling of graphene. In addition, on a

quasi-liquid substrate, the healing of defects is enhanced [20, 48, 49]. These mechanisms, acting above the onset of Ge surface melting, favor the formation of a flat, high-quality graphene film at high deposition temperature, as evidenced by Raman fingerprints (i.e. drop of D band intensity and increase of the I_{2D}/I_G ratio). Conversely, the graphene growing at lower T_D on a solid Ge surface needs to adapt to the uneven substrate corrugation: thus it develops strong ripple-like corrugations and, eventually, a higher concentration of defects.

We believe that the onset of surface melting, and its relationship with graphene quality, also affects the graphene relaxation dynamics while cooling from the deposition to room temperature hence the wrinkling. A requisite for wrinkles formation is that graphene can glide smoothly with little energetic expense on the substrate [44, 50]. This is indeed the case at high T_D where the corrugation in the Ge substrate smoothens out due to the onset of surface melting, favoring thermal strain relaxation by wrinkling in this regime.

Finally, we suggest that the nucleation of embryos graphene bilayer observed at $T_D=930^\circ$ is also in line with the formation of a quasi-liquid Ge surface layer which boosts the mobility of Ge atoms and their diffusional flow up to the surface of the first graphene layer, in line with what was observed on Ge(001) [13, 20].

Drawing a parallel between the data reported here for graphene/Ge(110) and the graphene synthesis Ge(001) [20], we deduce that the intimate connection of incomplete melting of Ge to the quality of graphene synthesis appears to be the general and leading driving force for quality enhancement of graphene on Ge substrates.

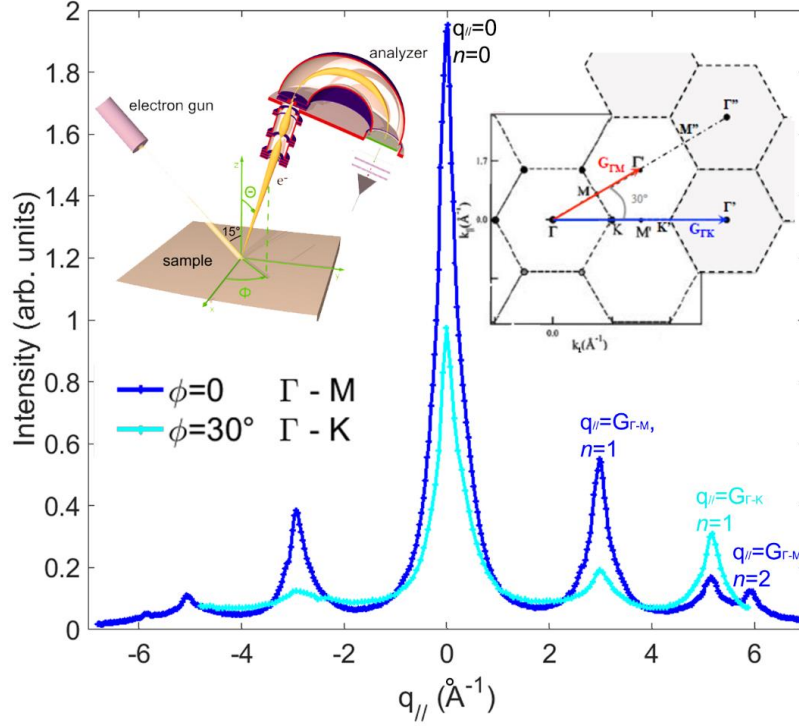


Fig. 4. LEED spectra acquired at different azimuthal orientations on the graphene sample grown at $T_D (= T_C) = 930$ °C. The experimental geometry is sketched in the inset together with the reciprocal-space map of a graphene lattice. The electron energy used was 72 eV.

Graphene nanoribbons

Our results demonstrate that adopting a pre-growth annealing to $T_C = 930$ °C the Ge substrate shows wide terraces, thus being potentially a suitable template for the growth of graphene nanostructures such as nanoribbons. In addition to a proper substrate morphology, the nanoribbon deposition also needs a lower growth rate [21] with respect to that we observed for T_D in the 910 -930 °C range. We then decoupled the effect of the Ge template morphology from the graphene growth process by exploring the condition $T_C \neq T_D$. To this end, we performed the pre-growth annealing of the Ge substrate at $T_C = 930$ °C and then performed the CVD deposition at $T_D = 890$ °C.

Following this recipe, STM images show the formation of graphene nanoribbons on the Ge(110) surface [Figs. 5(a), 5(b)]. Interestingly, the ribbons have widths of ~ 5 nm, thus entering the ultra-thin lateral-size

level required for high-performance digital electronics. Their length is typically above 40 nm and the height 3.3-3.6 Å, well matching the out-of-plane spacing of graphene/Ge(110)[10]. By inspecting the large-scale STM image in Fig. 5(a), it is evident that the alignment of the nanoribbons on Ge(110) is not stochastic. We find that the nanoribbon axis is aligned along specific high-symmetry directions of the Ge(110) surface, i.e. the [-112] and the [1-10] forming a relative angle of $\sim 54^\circ$ [33, 34]. Thanks to mirror symmetry of Ge(110) surface with respect to the [-110], the latter shows a twin orientation for $\sim 74^\circ$ azimuthal misorientation [32]. Indeed, we find that some ribbons grow along a direction forming an angle of $\sim 74^\circ$ with respect to the [-110] [Fig. 5(a)]. It is interesting to note that graphene islands with the armchair direction parallel to the [1-10] direction have been observed at the initial stage graphene growth on Ge(110) [10]. In addition, we note that the [-112] and the 74° -misaligned directions are also relevant for the graphene/Ge(110) interface, being related to the characteristic surface reconstruction of Ge(110) below graphene [33]. By performing high-resolution STM, we find that the ribbons show the typical electron scattering pattern of regular armchair edge termination [Fig. 5(c)], similarly to what observed on Ge(001)[21], while the Ge surface around the ribbons appears mostly oxidized after transfer *ex situ* to the STM chamber [inset of Fig. 5(b)]. Finally, it should be noted that the Ge substrate is mostly uncovered at this growth temperature, this indicating that the catalytic efficiency of Ge declines abruptly below 900 °C.

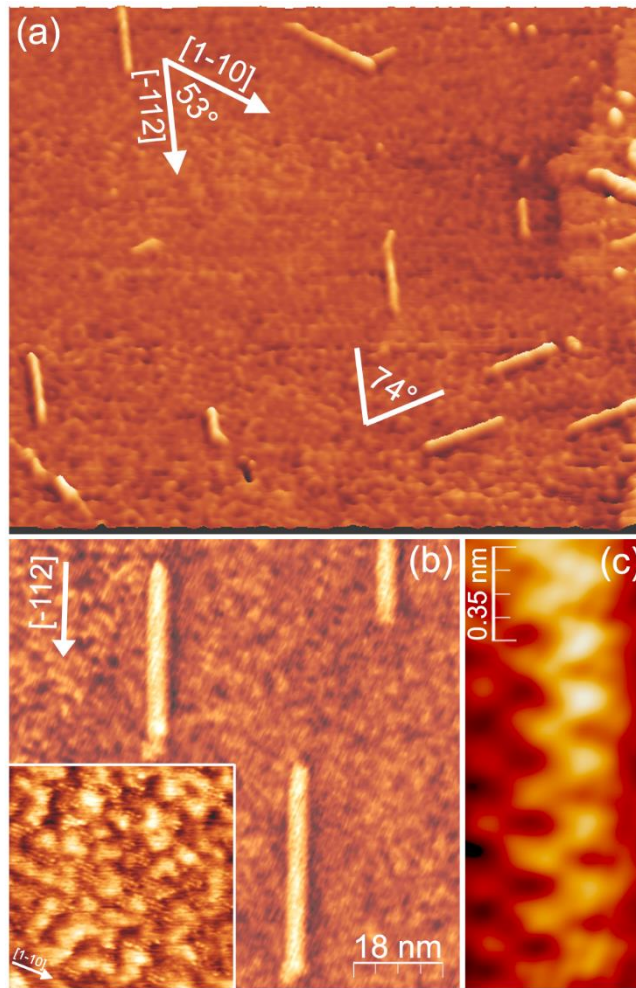


Fig. 5. *STM images of graphene nanoribbons grown at $T_C= 930$ °C and $T_D= 890$ °C. (a, b) ($U= -720$ mV, $I= 1.5$ nA). (c) Armchair edge of ribbons ($U= -300$ mV, $I= 1.7$ nA).*

4. Conclusions

In conclusion, we showed that both the deposition temperature of graphene and the annealing temperature during the cleaning step of Ge critically determine the results of CVD graphene growth on Ge(110). By a fine tuning of these temperatures, we triggered the synthesis of either a continuous graphene film or, for the first time on this Ge surface orientation, ultrathin armchair nanoribbons with widths ~ 5 nm. The quality of the continuous graphene film improves dramatically within a narrow range

of deposition temperatures only very close to the melting point of Ge, as expected in presence of an incomplete surface melting of the substrate. The results obtained demonstrate the versatility of the CVD synthesis of graphene on Ge(110) and the potential of this approach as a CMOS-compatible process.

Acknowledgements

The Lime Laboratory of Roma Tre University is acknowledged for technical support.

References

- [1] K.S. Novoselov, D. Jiang, F. Schedin, T.J. Booth, V.V. Khotkevich, S.V. Morozov, A.K. Geim, Two-dimensional atomic crystals, *Proc. Natl. Acad. Sci. U. S. A.*, 102 (2005) 10451-10453.
- [2] L.E.F. Torres, S. Roche, J.-C. Charlier, Introduction to Graphene-Based Nanomaterials: From Electronic Structure to Quantum Transport, *MRS Bulletin*, 40 (2015) 452-452.
- [3] A. Celis, M.N. Nair, A. Taleb-Ibrahimi, E.H. Conrad, C. Berger, W.A. de Heer, A. Tejeda, Graphene nanoribbons: fabrication, properties and devices, *J. Phys. D: Appl. Phys.*, 49 (2016) 143001.
- [4] J.-H. Lee, S.-G. Kang, H.-S. Jang, J.-Y. Moon, D. Whang, Graphene on Group-IV Elementary Semiconductors: The Direct Growth Approach and Its Applications, *Advanced Materials*, (2019) 1803469.
- [5] G. Lupina, J. Kitzmann, I. Costina, M. Lukosius, C. Wenger, A. Wolff, S. Vaziri, M. Östling, I. Pasternak, A. Krajewska, W. Strupinski, S. Kataria, A. Gahoi, M.C. Lemme, G. Ruhl, G. Zoth, O. Luxenhofer, W. Mehr, Residual Metallic Contamination of Transferred Chemical Vapor Deposited Graphene, *ACS Nano*, 9 (2015) 4776-4785.
- [6] D. Kosynkin, A. Higginbotham, A. Sinitskii, J. Lomeda, A. Dimiev, K. Price, J. Tour, Longitudinal unzipping of carbon nanotubes to form graphene nanoribbons, *Nature*, 458 (2009) 872-876.
- [7] F. Cataldo, G. Compagnini, G. Patané, O. Ursini, G. Angelini, P.R. Ribic, G. Margaritondo, A. Cricenti, G. Palleschi, F. Valentini, Graphene nanoribbons produced by the oxidative unzipping of single-wall carbon nanotubes, *Carbon*, 48 (2010) 2596-2602.
- [8] L. Persichetti, F. Tombolini, S. Casciardi, M. Diociaiuti, M. Fanfoni, G. Palleschi, A. Sgarlata, F. Valentini, A. Balzarotti, Folding and stacking defects of graphene flakes probed by electron nanobeam, *Appl. Phys. Lett.*, 99 (2011) 041904.
- [9] G. Wang, M. Zhang, Y. Zhu, G. Ding, D. Jiang, Q. Guo, S. Liu, X. Xie, P.K. Chu, Z. Di, X. Wang, Direct Growth of Graphene Film on Germanium Substrate, *Scientific Reports*, 3 (2013) 2465.

- [10] J.-H. Lee, E.K. Lee, W.-J. Joo, Y. Jang, B.-S. Kim, J.Y. Lim, S.-H. Choi, S.J. Ahn, J.R. Ahn, M.-H. Park, C.-W. Yang, B.L. Choi, S.-W. Hwang, D. Whang, Wafer-Scale Growth of Single-Crystal Monolayer Graphene on Reusable Hydrogen-Terminated Germanium, *Science*, 344 (2014) 286-289.
- [11] B. Kiraly, R.M. Jacobberger, A.J. Mannix, G.P. Campbell, M.J. Bedzyk, M.S. Arnold, M.C. Hersam, N.P. Guisinger, Electronic and Mechanical Properties of Graphene–Germanium Interfaces Grown by Chemical Vapor Deposition, *Nano Lett.*, 15 (2015) 7414-7420.
- [12] I. Pasternak, M. Wesolowski, I. Jozwik, M. Lukosius, G. Lupina, P. Dabrowski, J.M. Baranowski, W. Strupinski, Graphene growth on Ge(100)/Si(100) substrates by CVD method, *Scientific Reports*, 6 (2016) 21773.
- [13] A.M. Scaparro, V. Miseikis, C. Coletti, A. Notargiacomo, M. Pea, M. De Seta, L. Di Gaspare, Investigating the CVD Synthesis of Graphene on Ge(100): toward Layer-by-Layer Growth, *ACS Applied Materials & Interfaces*, 8 (2016) 33083-33090.
- [14] J. Dabrowski, G. Lippert, J. Avila, J. Baringhaus, I. Colambo, Y.S. Dedkov, F. Herziger, G. Lupina, J. Maultzsch, T. Schaffus, T. Schroeder, M. Kot, C. Tegenkamp, D. Vignaud, M.C. Asensio, Understanding the growth mechanism of graphene on Ge/Si(001) surfaces, *Scientific Reports*, 6 (2016) 31639.
- [15] J. Tesch, E. Voloshina, M. Fonin, Y. Dedkov, Growth and electronic structure of graphene on semiconducting Ge(110), *Carbon*, 122 (2017) 428-433.
- [16] I. Pasternak, P. Dabrowski, P. Ciepielewski, V. Kolkovskiy, Z. Klusek, J.M. Baranowski, W. Strupinski, Large-area high-quality graphene on Ge(001)/Si(001) substrates, *Nanoscale*, 8 (2016) 11241-11247.
- [17] P. Dabrowski, M. Rogala, I. Pasternak, J. Baranowski, W. Strupinski, M. Kopciuszynski, R. Zdyb, M. Jalochocki, I. Lutsyk, Z. Klusek, The study of the interactions between graphene and Ge(001)/Si(001), *Nano Research*, 10 (2017) 3648-3661.
- [18] L. Di Gaspare, A.M. Scaparro, M. Fanfoni, L. Fazi, A. Sgarlata, A. Notargiacomo, V. Miseikis, C. Coletti, M. De Seta, Early stage of CVD graphene synthesis on Ge(001) substrate, *Carbon*, 134 (2018) 183-188.
- [19] C.D. Mendoza, P.G. Caldas, F.L. Freire, M.E.H. Maia da Costa, Growth of single-layer graphene on Ge (1 0 0) by chemical vapor deposition, *Appl. Surf. Sci.*, 447 (2018) 816-821.
- [20] L. Persichetti, L. Di Gaspare, F. Fabbri, A.M. Scaparro, A. Notargiacomo, A. Sgarlata, M. Fanfoni, V. Miseikis, C. Coletti, M. De Seta, Abrupt changes in the graphene on Ge(001) system at the onset of surface melting, *Carbon*, 145 (2019) 345-351.
- [21] R.M. Jacobberger, B. Kiraly, M. Fortin-Deschenes, P.L. Levesque, K.M. McElhinny, G.J. Brady, R. Rojas Delgado, S. Singha Roy, A. Mannix, M.G. Lagally, P.G. Evans, P. Desjardins, R. Martel, M.C. Hersam, N.P. Guisinger, M.S. Arnold, Direct oriented growth of armchair graphene nanoribbons on germanium, *Nature Communications*, 6 (2015) 8006.

- [22] B. Kiraly, A.J. Mannix, R.M. Jacobberger, B.L. Fisher, M.S. Arnold, M.C. Hersam, N.P. Guisinger, Sub-5 nm, globally aligned graphene nanoribbons on Ge(001), *Appl. Phys. Lett.*, 108 (2016) 213101.
- [23] R.M. Jacobberger, M.S. Arnold, High-Performance Charge Transport in Semiconducting Armchair Graphene Nanoribbons Grown Directly on Germanium, *ACS Nano*, 11 (2017) 8924-8929.
- [24] A.J. Way, R.M. Jacobberger, M.S. Arnold, Seed-Initiated Anisotropic Growth of Unidirectional Armchair Graphene Nanoribbon Arrays on Germanium, *Nano Lett.*, 18 (2018) 898-906.
- [25] R.M. Jacobberger, E.A. Murray, M. Fortin-Deschênes, F. Göttl, W.A. Behn, Z.J. Krebs, P.L. Levesque, D.E. Savage, C. Smoot, M.G. Lagally, P. Desjardins, R. Martel, V. Brar, O. Moutanabbir, M. Mavrikakis, M.S. Arnold, Alignment of semiconducting graphene nanoribbons on vicinal Ge(001), *Nanoscale*, 11 (2019) 4864-4875.
- [26] K.M. McElhinny, R.M. Jacobberger, A.J. Zaugg, M.S. Arnold, P.G. Evans, Graphene-induced Ge (001) surface faceting, *Surf. Sci.*, 647 (2016) 90-95.
- [27] M. Lukosius, J. Dabrowski, J. Kitzmann, O. Fursenko, F. Akhtar, M. Lisker, G. Lippert, S. Schulze, Y. Yamamoto, M.A. Schubert, H.M. Krause, A. Wolff, A. Mai, T. Schroeder, G. Lupina, Metal-Free CVD Graphene Synthesis on 200 mm Ge/Si(001) Substrates, *ACS Applied Materials & Interfaces*, 8 (2016) 33786-33793.
- [28] L. Persichetti, A. Sgarlata, M. Fanfoni, A. Balzarotti, Irreversible order-disorder transformation of Ge(001) probed by scanning tunnelling microscopy, *J. Phys.: Condens. Matter*, 27 (2015) 435001.
- [29] L. Persichetti, M. Fanfoni, B. Bonanni, M. De Seta, L. Di Gaspare, C. Goletti, L. Ottaviano, A. Sgarlata, Islanding, growth mode and ordering in Si heteroepitaxy on Ge(001) substrates structured by thermal annealing, *Surf. Sci.*, 683 (2019) 31-37.
- [30] L. Persichetti, A. Sgarlata, M. Fanfoni, A. Balzarotti, Heteroepitaxy of Ge on singular and vicinal Si surfaces: elastic field symmetry and nanostructure growth, *J. Phys.: Condens. Matter*, 27 (2015) 253001.
- [31] J. Tesch, F. Paschke, M. Fonin, M. Wietstruk, S. Böttcher, R.J. Koch, A. Bostwick, C. Jozwiak, E. Rotenberg, A. Makarova, B. Paulus, E. Voloshina, Y. Dedkov, The graphene/n-Ge(110) interface: structure, doping, and electronic properties, *Nanoscale*, 10 (2018) 6088-6098.
- [32] H.W. Kim, W. Ko, W.-J. Joo, Y. Cho, Y. Oh, J. Ku, I. Jeon, S. Park, S.W. Hwang, Unraveling the Structural and Electronic Properties of Graphene/Ge(110), *The Journal of Physical Chemistry Letters*, 9 (2018) 7059-7063.
- [33] D. Zhou, Z. Niu, T. Niu, Surface Reconstruction of Germanium: Hydrogen Intercalation and Graphene Protection, *The Journal of Physical Chemistry C*, 122 (2018) 21874-21882.
- [34] G.P. Campbell, B. Kiraly, R.M. Jacobberger, A.J. Mannix, M.S. Arnold, M.C. Hersam, N.P. Guisinger, M.J. Bedzyk, Epitaxial graphene-encapsulated surface reconstruction of Ge(110), *Physical Review Materials*, 2 (2018) 044004.

- [35] B. Kiraly, A.J. Mannix, R.M. Jacobberger, B.L. Fisher, M.S. Arnold, M.C. Hersam, N.P. Guisinger, Driving chemical interactions at graphene-germanium van der Waals interfaces via thermal annealing, *Appl. Phys. Lett.*, 113 (2018) 213103.
- [36] J. Dai, D. Wang, M. Zhang, T. Niu, A. Li, M. Ye, S. Qiao, G. Ding, X. Xie, Y. Wang, P.K. Chu, Q. Yuan, Z. Di, X. Wang, F. Ding, B.I. Yakobson, How Graphene Islands Are Unidirectionally Aligned on the Ge(110) Surface, *Nano Lett.*, 16 (2016) 3160-3165.
- [37] P.C. Rogge, M.E. Foster, J.M. Wofford, K.F. McCarty, N.C. Bartelt, O.D. Dubon, On the rotational alignment of graphene domains grown on Ge(110) and Ge(111), *MRS Communications*, 5 (2015) 539-546.
- [38] E.H. Martins Ferreira, M.V.O. Moutinho, F. Stavale, M.M. Lucchese, R.B. Capaz, C.A. Achete, A. Jorio, Evolution of the Raman spectra from single-, few-, and many-layer graphene with increasing disorder, *Phys. Rev. B*, 82 (2010) 125429.
- [39] P. Venezuela, M. Lazzeri, F. Mauri, Theory of double-resonant Raman spectra in graphene: Intensity and line shape of defect-induced and two-phonon bands, *Phys. Rev. B*, 84 (2011) 035433.
- [40] L.G. Cançado, A. Jorio, E.H.M. Ferreira, F. Stavale, C.A. Achete, R.B. Capaz, M.V.O. Moutinho, A. Lombardo, T.S. Kulmala, A.C. Ferrari, Quantifying Defects in Graphene via Raman Spectroscopy at Different Excitation Energies, *Nano Lett.*, 11 (2011) 3190-3196.
- [41] J.E. Lee, G. Ahn, J. Shim, Y.S. Lee, S. Ryu, Optical separation of mechanical strain from charge doping in graphene, *Nature Communications*, 3 (2012) 1024.
- [42] O.T. Ogurtani, D. Senyildiz, G. Cambaz Buke, Wrinkling of graphene because of the thermal expansion mismatch between graphene and copper, *Surf. Interface Anal.*, 50 (2018) 547-551.
- [43] V.K. Yang, M. Groenert, C.W. Leitz, A.J. Pitera, M.T. Currie, E.A. Fitzgerald, Crack formation in GaAs heteroepitaxial films on Si and SiGe virtual substrates, *J. Appl. Phys.*, 93 (2003) 3859-3865.
- [44] H. Hattab, A.T. N'Diaye, D. Wall, C. Klein, G. Jnawali, J. Coraux, C. Busse, R. van Gastel, B. Poelsema, T. Michely, F.-J. Meyer zu Heringdorf, M. Horn-von Hoegen, Interplay of Wrinkles, Strain, and Lattice Parameter in Graphene on Iridium, *Nano Lett.*, 12 (2012) 678-682.
- [45] H.S. Wong, C. Durkan, Unraveling the rotational disorder of graphene layers in graphite, *Phys. Rev. B*, 81 (2010) 045403.
- [46] U. Tartaglino, T. Zykova-Timan, F. Ercolessi, E. Tosatti, Melting and nonmelting of solid surfaces and nanosystems, *Phys. Rep.*, 411 (2005) 291-321.
- [47] P.C. Rogge, K. Thürmer, M.E. Foster, K.F. McCarty, O.D. Dubon, N.C. Bartelt, Real-time observation of epitaxial graphene domain reorientation, *Nature Communications*, 6 (2015) 6880.
- [48] T. Niu, M. Zhou, J. Zhang, Y. Feng, W. Chen, Growth intermediates for CVD graphene on Cu(111): carbon clusters and defective graphene, *J. Am. Chem. Soc.*, 135 (2013) 8409-8414.

[49] H.-B. Li, A.J. Page, C. Hettich, B. Aradi, C. Köhler, T. Frauenheim, S. Irle, K. Morokuma, Graphene nucleation on a surface-molten copper catalyst: quantum chemical molecular dynamics simulations, *Chemical Science*, 5 (2014) 3493-3500.

[50] Z. Pang, B. Deng, Z. Liu, H. Peng, Y. Wei, Defects guided wrinkling in graphene on copper substrate, *Carbon*, 143 (2019) 736-742.